

1 Intrinsic dynamic shapes responses to external stimulation 2 in the human brain

3

4 Maximilian Nentwich¹, Marcin Leszczynski^{2,3,4}, Charles E. Schroeder^{2,3}, Stephan Bickel^{1,5,6},
5 Lucas C. Parra⁷

6

7 ¹ The Feinstein Institutes for Medical Research, Northwell Health, Manhasset, NY, USA;

8 ² Departments of Psychiatry and Neurology, Columbia University College of Physicians and Surgeons,
9 New York, NY, USA;

10 ³ Translational Neuroscience Lab Division, Center for Biomedical Imaging and Neuromodulation, Nathan
11 Kline Institute, Orangeburg, NY, USA;

12 ⁴ Cognitive Science Department, Institute of Philosophy, Jagiellonian University, Kraków, Poland;

13 ⁵ Departments of Neurology and Neurosurgery, Zucker School of Medicine at Hofstra/Northwell,
14 Hempstead, NY, USA;

15 ⁶ Center for Biomedical Imaging and Neuromodulation, Nathan Kline Institute, Orangeburg, NY, USA;

16 ⁷ Department of Biomedical Engineering, The City College of New York, New York, NY, USA

17

18

19 Summary

20

21 Sensory stimulation of the brain reverberates in its recurrent neuronal networks. However,
22 current computational models of brain activity do not separate immediate sensory responses
23 from intrinsic recurrent dynamics. We apply a vector-autoregressive model with external input
24 (VARX), combining the concepts of “functional connectivity” and “encoding models”, to
25 intracranial recordings in humans. We find that the recurrent connectivity during rest is largely
26 unaltered during movie watching. The intrinsic recurrent dynamic enhances and prolongs the
27 neural responses to scene cuts, eye movements, and sounds. Failing to account for these
28 exogenous inputs, leads to spurious connections in the intrinsic “connectivity”. The model shows
29 that an external stimulus can reduce intrinsic noise. It also shows that sensory areas have
30 mostly outward, whereas higher-order brain areas mostly incoming connections. We conclude
31 that the response to an external audiovisual stimulus can largely be attributed to the intrinsic
32 dynamic of the brain, already observed during rest.

33

34

35 Keywords

36

37 Connectivity, Granger analysis, VAR, recurrent networks, encoding models, intracranial EEG,
38 eye movements, naturalistic

39 Introduction

40

41 The primate brain is highly interconnected between and within brain areas. This includes areas
42 involved in sensory processing ¹. Strikingly, most computational models of brain activity in
43 response to external natural stimuli do not take the recurrent architecture of brain networks into
44 account. "Encoding" models often rely on simple input/output relationships such as general
45 linear models in fMRI ², or temporal response functions in EEG/MEG ³. Interactions between
46 brain areas are captured often just as instantaneous linear correlations that are referred to as
47 "functional connectivity" when analyzing fMRI activity ⁴. Others capture synchronous activity in
48 different brain areas by measuring phase locking of electrical neural signals ⁵. However, these
49 measures of instantaneous correlation do not capture time delays inherent in recurrent
50 dynamics. By taking temporal precedence into account with recurrent models the
51 "Granger-causality" formalism can establish directed "connectivity". This has been used to
52 analyze both fMRI and electrical activity ⁶⁻¹¹.

53

54 The concept of functional connectivity was first developed to analyze neural activity during rest,
55 where there are no obvious external signals to stimulate brain activity. But it is now also often
56 used during passive exposure to a stimulus, such as watching movies ¹²⁻¹⁵. A general
57 observation of these studies is that a portion of the functional connectivity is preserved between
58 rest and stimulus conditions, while some aspects are altered by the perceptual task, e.g. ^{12,16}.
59 This should be no surprise, given that an external stimulus can drive multiple brain areas and
60 thus induce correlations between these areas ¹⁷. Removing such stimulus-induced correlations
61 by controlling for a common cause is standard practice in statistical modeling and causal
62 inference ¹⁸. However, in studies that focus on functional connectivity in neuroscience,
63 stimulus-induced correlations are often ignored when analyzing the correlation structure of
64 neural signals. A notable exception is "dynamic causal modeling" ¹⁹. In this modeling approach
65 the "input" can modulate functional connectivity. This is particularly important in the context of
66 active behavioral tasks, where the common finding is that correlation structure changes with
67 task states ²⁰.

68

69 In this study we are interested in "passive" tasks such as rest and movie watching. We will ask
70 here whether, after removing stimulus-induced correlations, the intrinsic dynamic itself is
71 preserved. Attempts to factor out the effects of the stimulus come from work on response
72 variability. For instance, fMRI shows that variability across trials in motor cortex is due to an
73 intrinsic "noise" which is linearly superimposed on a more reliable response to a simple motor
74 action ²¹. Stimulus-response variability in the visual cortex has been attributed to variability of
75 ongoing dynamic ^{22,23}. Some studies of electrical recordings from the visual cortex show that
76 correlations of spiking activity between different recording locations are largely unaffected by
77 visual stimulation ²⁴. Yet, other studies show that visual input affects local correlation in the
78 visual cortex ²⁵⁻²⁷ and across the brain ²⁸.

79

80 The technical challenge when addressing these questions is to separate the direct effect of the
81 stimulus from the intrinsic recurrent dynamic. Here we propose to separate these effects by
82 modeling them simultaneously with the simplest possible model, namely, linear intrinsic effects

83 between brain areas and linear responses to extrinsic input. A mathematical model that
84 implements this is the vector-autoregressive model with external input (VARX). This model is
85 well established in the field of linear systems²⁹ and econometrics³⁰, where it is used to capture
86 intrinsic dynamics in the presence of an external input. The VARX model is an extension of the
87 VAR model that is routinely used to establish "Granger-causality" in neuroscience (cited above).
88 In the VARX model, Granger analysis provides a measure of statistical significance for the
89 intrinsic dynamic as well as the external input, in addition to directionality for the intrinsic effects,
90 all as part of a single model³¹.

91

92 While linear systems are an inadequate model of neuronal dynamics, they remain an important
93 tool to understand neural representations because of their conceptual simplicity. They are
94 routinely used for event-related fMRI analysis but also for "encoding models" to link non-linear
95 features of continuous stimuli to neural responses. They have been used to analyze responses
96 to video in fMRI³², to speech in EEG³³ or to audio in intracranial EEG³⁴. They are even used to
97 analyze the encoding in deep-neural network models³⁵. Here we use a classic linear model to
98 combine two canonical concepts in neuroscience, which have thus far remained separated,
99 namely, that of "encoding models"³² and "functional connectivity" models⁶. We will use this to
100 analyze whole-brain, intracranial EEG in human subjects at rest, and while they watch videos.
101 Our main finding is that the recurrent dynamic observed during rest is only minimally altered by
102 watching videos. Instead, the brain's response to naturalistic stimulus appears to be
103 substantially shaped by the same endogenous dynamic of the brain observed during rest.

104

105

106 **Methods**

107

108 The vector-autoregressive model with external input (VARX) falls within a group of
109 well-established linear models used in neuroscience (see Table 1). Prominent examples in this
110 group are the generalized linear model (GLM), dynamic causal model (DCM) and temporal
111 response functions (TRF). While these models have been extensively used for neural signal
112 analysis, the VARX model has not. We start therefore with a brief introduction. For more details
113 please refer to³¹

114

115

116 ***VARX model***

117

118 The VARX model explains a time-varying vectorial signal $y(t)$ as the result of an intrinsic
119 autoregressive feedback driven by an innovation process $e(t)$ and an extrinsic¹ input $x(t)$:

120

$$121 \mathbf{y}(t) = \mathbf{A} * \mathbf{y}(t - 1) + \mathbf{B} * \mathbf{x}(t) + \mathbf{e}(t)$$

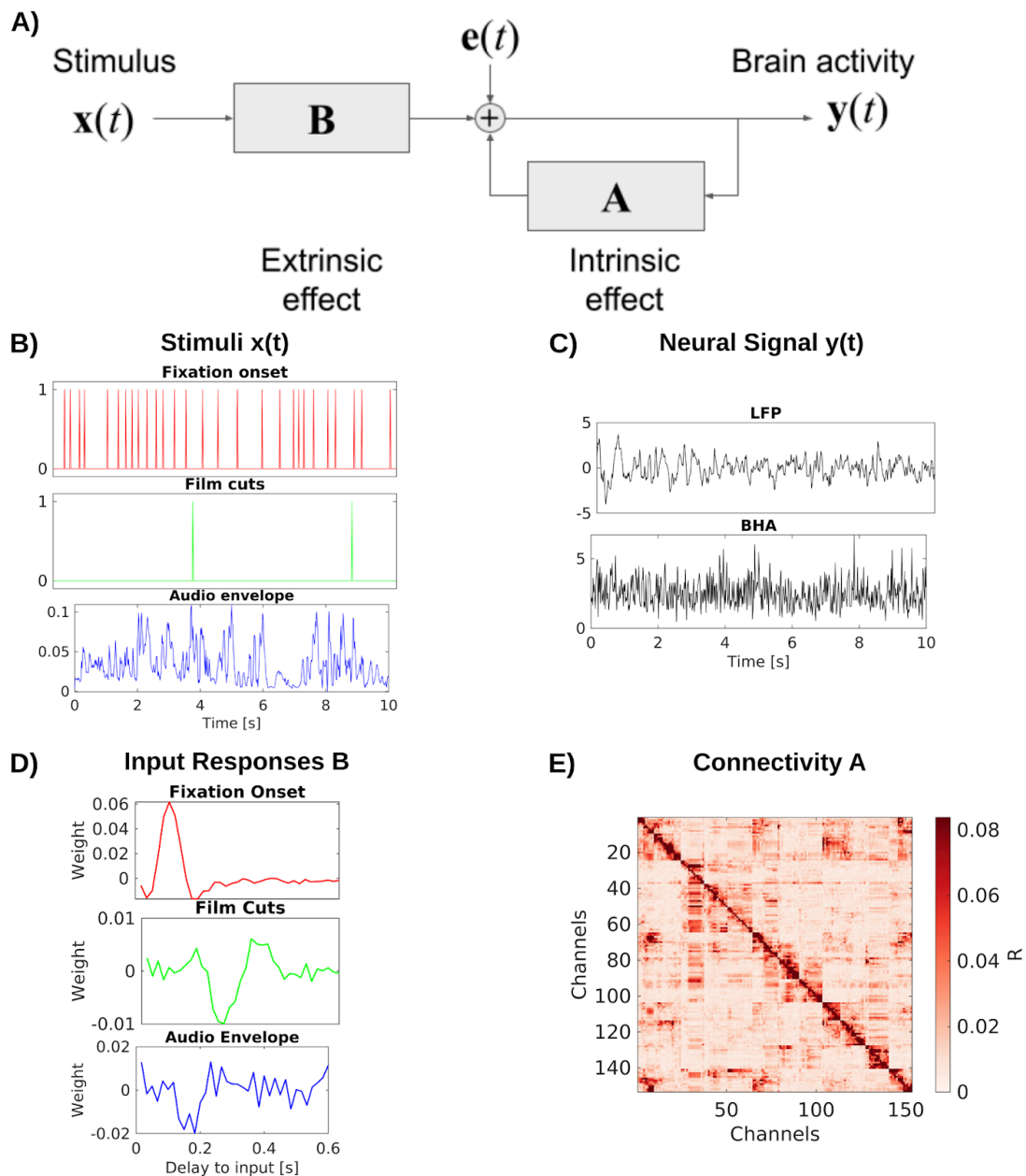
122

123 ¹ We adopt here the terminology of "intrinsic" and "extrinsic" as it is commonly used in neuroscience and
124 psychology. In system modeling and econometrics, where the VARX model is prevalent, the more
125 common terminology is "endogenous" and "exogenous", meaning effectively the same thing.

126 \mathbf{A}^* and \mathbf{B}^* represent convolutions with appropriately sized matrices of causal filters with
 127 lengths n_a and n_b respectively. The innovation is assumed to be uncorrelated in time and has
 128 therefore a uniform spectrum. The recurrence in \mathbf{A} modifies this spectrum to match the spectrum
 129 of $y(t)$, thereby capturing the intrinsic recurrent dynamic. The filter \mathbf{B} injects a filtered version
 130 of the extrinsic input $x(t)$ into this recurrent dynamic. The role of each of these terms for brain
 131 activity is explained in Fig. 1.

132

133



134

135 **Figure 1: VARX model of the brain:** A) Block diagram of VARX model. $y(t)$ represents observable
 136 neural activity in different brain areas, $x(t)$ are observable features of a continuous sensory stimulus, \mathbf{A}
 137 represent the recurrent connections within and between brain areas (intrinsic effect), and \mathbf{B} captures the

138 transduction of the sensory stimuli into neural activity and transmission to different brain areas (extrinsic
139 effect). The diagonal term in \mathbf{A} captures recurrent feedback within a brain area. Finally, $\mathbf{e}(t)$ is
140 unobserved intrinsic “random” brain activity. B) Example of input stimulus features $\mathbf{x}(t)$. C) Single channel
141 examples of neural signal $y(t)$. D) Examples of moving-average response filters \mathbf{B} . E) Effect size R for
142 the “connections” captured by auto-regressive filters \mathbf{A} .

143

144 Filter matrices \mathbf{A} and \mathbf{B} are unknown and can be estimated from the observed history of $\mathbf{x}(t)$
145 and $y(t)$ using ordinary least squares (OLS). The objective for the optimal model is to minimize
146 the power of the unobserved innovation process $\mathbf{e}(t)$:

$$\sigma^2 = 1/T \sum_{t=1}^T \mathbf{e}(t)^2$$

147

148

149 **Granger analysis**

150

151 The innovation is also the prediction error, for predicting $y(t)$ from the past $y(t-1)$ and input
152 $\mathbf{x}(t)$. In the Granger formalism the prediction error is calculated with all predictors included
153 (error of the full model, σ_f) or with individual dimension in $y(t-1)$ or $\mathbf{x}(t)$ omitted (error of the
154 reduced models, σ_r)³⁶. To quantify the “effect” of the specific dimension one can take the ratio
155 of these errors³⁷ leading to the test statistic D known as the “deviance”. When the number of
156 samples T is large, the deviance follows the Chi-square distribution with cumulative density F ,
157 from which one can compute a p-value:

158

$$D = T \log(\sigma_r^2 / \sigma_f^2)$$

159

160

161

162

163 The p-value quantifies the probability that a specific connection in \mathbf{A} or \mathbf{B} is zero. The
164 “generalized” R^2 ³⁸ serves as a measure of effect size, capturing the strength of each
165 connection (D , p and R can be computed for each connection in matrix \mathbf{A} or \mathbf{B}). While this
166 Granger formalism is well established in the context of estimating \mathbf{A} , i.e. VAR models, to our
167 knowledge, it has not been used in the context of estimating \mathbf{B} , i.e. VARX or TRF models.

168

169

170 **Overall system response**

171

172 The overall brain response to the stimulus for the VARX model is given by the system impulse
173 response (written here in the z -domain, or Fourier domain):

$$174 \mathbf{H} = (1 - \mathbf{A})^{-1} \mathbf{B}$$

175 What we see here is that the system response \mathbf{H} is factorized into an autoregressive (AR) filter
176 \mathbf{A} and a moving average (MA) filter \mathbf{B} . When modeled as a single MA filter, the total system
177 response has been called the “multivariate Temporal Response Function” (mTRF) in the

178 neuroscience community³⁹. We found that the VARX estimate of \mathbf{H} is nearly identical to the
179 estimated mTRF³¹. In other words, \mathbf{B} and \mathbf{A} are a valid factorization of the mTRF into
180 immediate extrinsic versus recurrent intrinsic effects.

181

182 Note that the extrinsic effects captured with filters \mathbf{B} are specific (every stimulus dimension has
183 a specific effect on each brain area), whereas the endogenous dynamic propagates this initial
184 effect to all connected brain areas via matrix \mathbf{A} , effectively mixing and adding the responses of
185 all stimulus dimensions. Therefore, this factorization separates stimulus-specific effects from the
186 shared endogenous dynamic.

187

188

189 ***Relation to common neural signal models***

190

191 The VARX model fits naturally into the existing family of models used for neural signals analysis
192 (Table 1). While they differ in the formulation and statistical assumptions, their defining
193 equations have a similar general form with the following attributes:

194

195 Table 1: Models commonly used in neural signal analysis

Model	Intrinsic effect \mathbf{A}	Extrinsic effect \mathbf{B}	Interact	Delay n_a, n_b	Estimation speed	Reference, with code where available
GLM	no	yes	no	=1	medium	⁴⁰ , SPM, FSL
DCM	yes	yes	yes ²	=1 ³	slow	¹⁹ , no code
VAR	yes	no	no	>1	fast/slow	⁴¹
mTRF	no	yes	no	>1	fast	³⁹
VARX	yes	yes	no ⁴	>1	fast	³¹

196

197 An important simplifying assumption for the mTRF, VAR, and VARX models is that $\mathbf{y}(t)$ is
198 observable with additive normal distributed innovation. As a result, parameter estimation can
199 use ordinary least squares, which is fast to compute. In contrast, GLM, DCM, and some variants
200 of VAR models assume that $\mathbf{y}(t)$ is not directly observable, and needs to be estimated in addition
201 to the unknown parameters \mathbf{A} or \mathbf{B} . The same is true for the basic “output error” model in
202 linear systems theory²⁹. This requires slower iterative algorithms, such as expectation
203 maximization. As a result, these models are often limited to small networks⁵ of a few nodes to
204 test specific alternative hypotheses⁴². In contrast, here we will analyze 100-200 channels per
205 subject to draw general conclusions about overall brain organization.

206

207

208

214 ² “Interact” refers to an additional bilinear interaction term of the form $\mathbf{x} \mathbf{C} \mathbf{y}$ that allows for a modulation of
215 intrinsic effect by the external input.

213 ³ The DCM is defined in terms of the first derivative of $\mathbf{y}(t)$, which in discret time is the same as $n_a=1$.

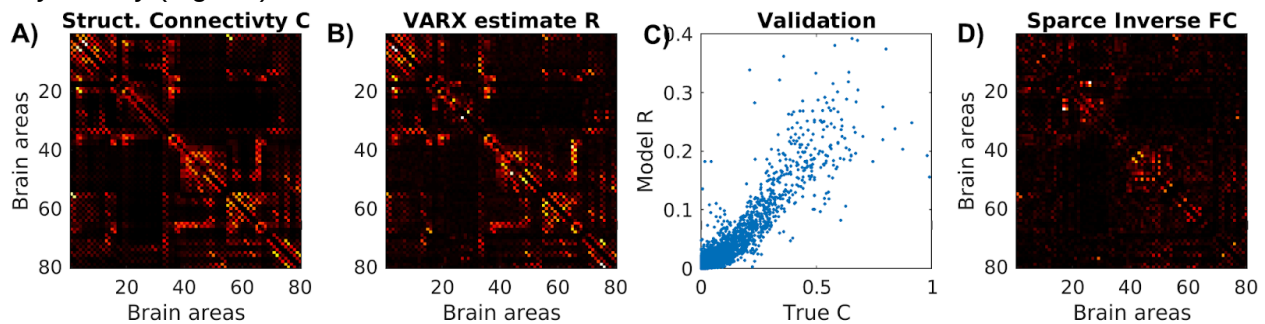
212 ⁴ It is straightforward to add an interaction term to the VARX model and maintain fast OLS estimation.

209 ⁵ The original DCM proposed for fMRI included an added complication of modeling the hemodynamic
210 response, which amounts to adding a temporal filter to each output node and prior to adding observation
211 noise.

216 **Validation of connectivity estimate on whole-brain neural mass model**

217

218 To validate the interpretation that \hat{A} is a model of “connectivity”, we simulated neural activity for
219 a whole-brain neural mass model⁴³. We used the default model of the neurolib python library
220 (“ALNModel”), which is a mean-field approximation of adaptive exponential integrate-and-fire
221 neurons. This model can generate simulated mean firing rates in 80 brain areas based on
222 connectivity and delay matrices determined with diffusion tensor imaging (DTI). We used 5 min
223 of “resting state” activity (no added stimulus, simulated at 0.1ms resolution, subsequently
224 downsampled to 100Hz). The true connectivity matrix from DTI (Fig. 2A) appears to be similar to
225 the effect size estimate R for the recurrent connections \hat{A} in the VARX model with no input (Fig.
226 2B). Following⁴⁴ we compare the two as a scatter plot (Fig. 2C) and observed a Spearman
227 correlation of 0.69. For comparison, we also used the sparse-inverse covariance method to
228 recover structural connectivity from functional connectivity. This method is more sensitive than
229 others in detecting network connections⁴⁵ and uses the graphical lasso algorithm⁴⁶. The
230 resulting connectivity estimate (Fig. 2D) only achieves a Spearman correlation of 0.52. We note
231 that the structural connectivity determined with DTI is largely symmetric. When enhancing the
232 asymmetry the VARX model is not as accurate, but correctly recovers the direction of the
233 asymmetry (Fig. S1).



235 **Figure 2: Connectivity of stimulated neural mass model for the whole brain, and estimated VARX**
236 **model.** A) True structural connectivity used to simulate neural activity using a neural mass model with the
237 neurolib python toolbox. Connectivity is based on diffusion tensor imaging data between 80 brain areas
238 (called Cmat in neurolib). Here showing the square root of the “Cmat” matrix for better visibility of small
239 connectivity values. B) Effect size estimate R for the \hat{A} matrix of the VARX model on the simulated data.
240 C) Comparison of true and VARX estimate of connectivity. D) Absolute value of the sparse-inverse
241 functional connectivity (estimated using graphical lasso⁴⁷).

242

243

244 **Intracranial EEG recordings and stimulus features**

245

246 We analyzed intracranial EEG and simultaneous eye-tracking data recorded from patients
247 (N=21, mean age 37.81 years, age range 19-58 years, 9 female, Table S1) during rest and
248 while they watched various video clips. Three patients underwent two implantations and
249 recordings at different times resulting in a total of 24 recording sessions with a total of 4,962
250 recording channels. The video clips included animations with speech (‘Despicable Me’, two
251 different clips, 10 min each, in English and Hungarian), an animated short film with a mostly
252 visual narrative and music, shown twice (‘The Present’, 4.3 min), and three clips of

253 documentaries of macaques ('Monkey', 5 min each, without sound) ⁴⁸. In addition to the clips
254 from the previous analysis, we included a movie clip of abstract animations ('Inscapes', 10 min)
255 ⁴⁹, and an eyes-open resting state with maintained fixation ('Resting state', 5 min). In total, we
256 recorded up to 59.3 minutes of data for each patient (Table S1). Two patients did not complete
257 both movie watching and resting state (Pat_5 & Pat_16) and were not included in the analysis
258 that compares the two conditions.

259

260 Neural signals were preprocessed as previously described to reduce noise ⁴⁸. We re-reference
261 signals in a bipolar montage to ensure analysis of local activity. We analyze local field potentials
262 (LFPs) and broadband high-frequency activity (BHA) power. BHA is the power of the signal
263 bandpass filtered between 70-150Hz. We perform analysis on both signals after downsampling
264 to 60Hz. Example traces of $y(t)$ for LFP and BHA are shown in Fig. 1B&C.

265

266 We extract three features of the movies that serve as external inputs for the VARX model:
267 fixation onset, film cuts and sound envelope (Fig. 3G). Fixation onset and film cuts are
268 represented in $x(t)$ as pulse trains with pulses occurring at the time of these events ⁴⁸. Sound
269 envelope is computed as the absolute value of the Hilbert transform of the sound from the
270 movie files and varies continuously. The envelope is downsampled to 60 Hz. All videos and
271 resting state include fixations. The video 'Inscapes' and resting state do not include film cuts as
272 external input. The 'Monkey' video clips and resting state do not include the sound envelope as
273 input features, but do include fixation onsets. When a feature is not available it is replaced with
274 features from a different recording. Therefore, the statistics of the feature are consistent, but not
275 aligned to the neural recording. When comparing models with different features we always keep
276 the number of input variables consistent between models to avoid a bias by the number of free
277 parameters of the model. Features that are not considered in the analysis are shuffled in time by
278 a circular shift by half the duration of the signals.

279

280 The VARX models were fitted to data with the matlab version of the code ³¹. For all analyses we
281 use filters of 600 ms length for inputs ($n_b=36$ samples for VARX models, $L=36$ samples for
282 mTRFmodels). Delays for connections between channels are set to 100ms ($n_a=6$ samples) for
283 both LFP and BHA signals. Increasing the number of delays n_a , increases estimated effect size
284 \bar{R} , however, larger values lead to overfitting, i.e. less significant connections (Fig. S1). Values
285 around $n_a=6$ samples achieve a balance between goodness of fit and overfitting (Fig. S2). The
286 regularization parameter was set to $\lambda=0.3$.

287

288 Connectivity plots are created with nilearn's `plot_connectome()` function (Fig. 4) ⁵⁰. We plot only
289 significant connections ($p<0.001$). Surface plots of T1w/T2w ratios and directionality of
290 connections are created using the field-echos repository ^{51,52}. T1w/T2w maps ⁵³ are obtained
291 from the neuromaps repository ^{54,55}, and transformed to the freesurfer surface using the
292 `fslr_to_fsaverage()` function ^{56,57}.

293

294 The length of responses for Fig. 5 is computed as the 'peak widths' argument of Matlab's
295 `findpeaks()` function. Power is computed as the average of the instantaneous power, i.e. the
296 square of the weight at each delay of the filters.

297 **Data and code availability**

298

299 The raw data reported in this study cannot be deposited in a public repository because of
300 patient privacy concerns. To request access, contact The Feinstein Institutes for Medical
301 Research, through Dr. Stephan Bickel. In addition, processed datasets derived from these data
302 have been deposited at <https://doi.org/10.17605/OSF.IO/VC25T> and are publicly available as of
303 the date of publication.

304

305 All original code has been deposited at https://github.com/MaxNentwich/varx_demo and is
306 publicly available at [DOI to be created with final version of code] as of the date of publication.

307

308

309 **Results**

310

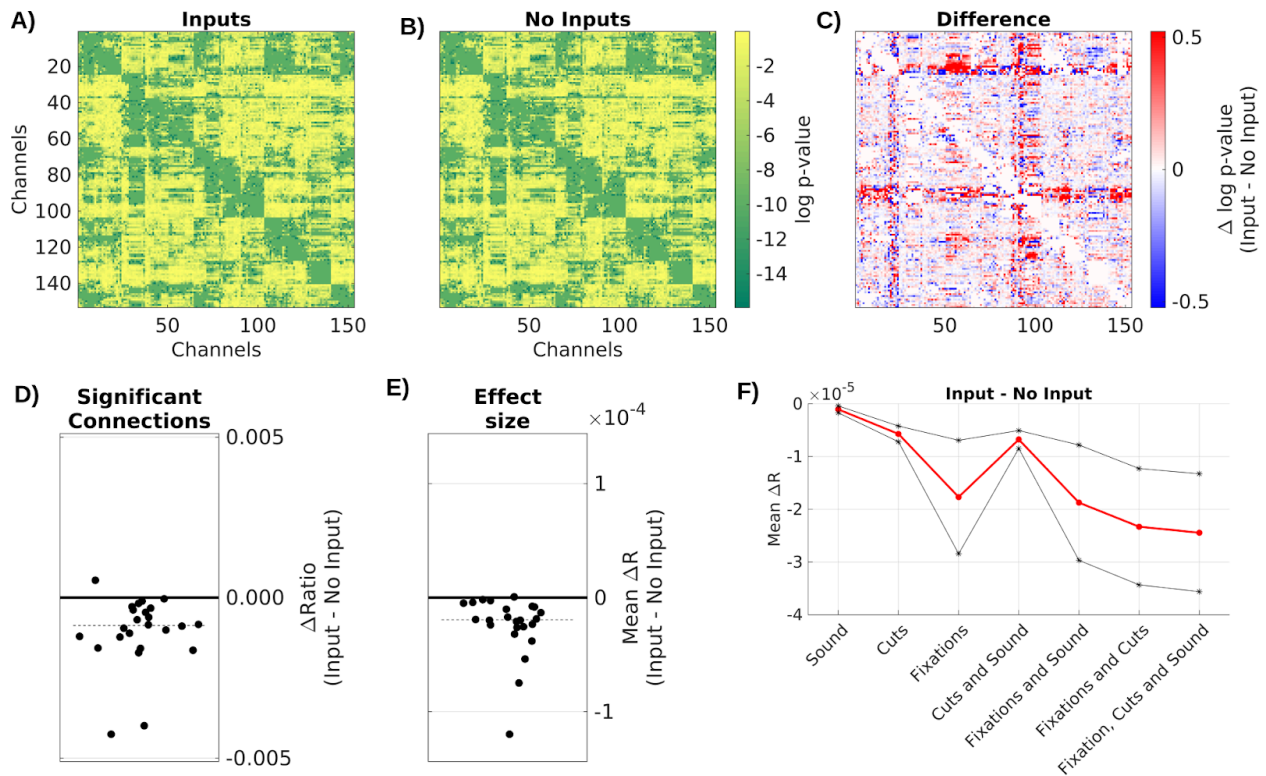
311 ***Extrinsic input leads to spurious intrinsic connectivity***

312

313 To determine the effect of the extrinsic inputs on connectivity estimates we either fit a VARX
314 model or a VAR model (i.e. a VARX model with no external input). We analyze LFP data on all
315 available recordings, movies and resting state for all N=24 recording sessions. As extrinsic
316 inputs we included film cuts, fixation onset, and sound envelope. VAR models contain the same
317 external inputs as the VARX model, but the time alignment is disrupted by a circular shuffle. This
318 keeps the number of parameters in different models constant and ensures the inputs have the
319 same covariance structure. We found a similar connectivity structure for the estimated VAR and
320 VARX models (Fig. 3A and 3B). However, they vary systematically in the number of significant
321 recurrent connections \mathbf{A} (those with $p < .0001$, Fig. 3D), which drops when adding inputs
322 (median = -8.7×10^{-4} , $p < .0001$, N=24, Wilcoxon). The effect sizes R also significantly decreases in
323 the VARX model (Fig. 3E, median = -1.9×10^{-5} , $p < .0001$, N=24, Wilcoxon). Therefore, accounting
324 for the external input removes spurious “connections”. We also analyzed how much each of
325 these inputs contributed to this effect (Fig. 3F). Out of the three input features considered,
326 models including fixations and cuts decrease effect size more than models with sound envelope
327 (fixations vs. sound, median $\Delta R = -1.0 \times 10^{-5}$, $p < .0001$, N=24; cuts vs. sound: median $\Delta R = -3.8 \times 10^{-6}$,
328 $p < .0001$, N=24; Wilcoxon, uncorrected). The model including the combination of all three
329 features has a smaller effect size R for \mathbf{A} than models with any individual input feature (all vs.
330 fixations: median $\Delta R = -6.5 \times 10^{-6}$, $p < .0001$, N=24; all vs. cuts: median $\Delta R = -1.2 \times 10^{-5}$, $p < .0001$,
331 N=24; all vs. sound: median $\Delta R = -1.9 \times 10^{-5}$, $p < .0001$, N=24; Wilcoxon, uncorrected). Thus, adding
332 more input features further reduces the strength of intrinsic “connections”. These results are
333 also reflected in the analysis of BHA signals (Fig. S3).

334

335



336

337 **Figure 3: Spurious intrinsic connectivity in A is removed when modeling the effect of exogenous**
 338 **input with B.** Comparison of VARX model with and without inputs. A) P -values for each connection in
 339 A for VARX model with inputs on one subject (Pat_1); B) for VARX model without inputs; C) difference.
 340 Both models are fit to the same data. D) Difference of fraction of significant recurrent connections
 341 between VARX models with and without inputs. E) Mean difference in R over all electrodes between
 342 VARX models with and without inputs. Each point is a subject. Dashed line is the median across subjects.
 343 F) Difference between the VARX models with different input combinations and the VARX model without
 344 inputs. Red line shows mean across patients, black lines the 95% confidence interval. Negative values
 345 indicate a decrease in connectivity strength when exogenous input is accounted for.

346

347

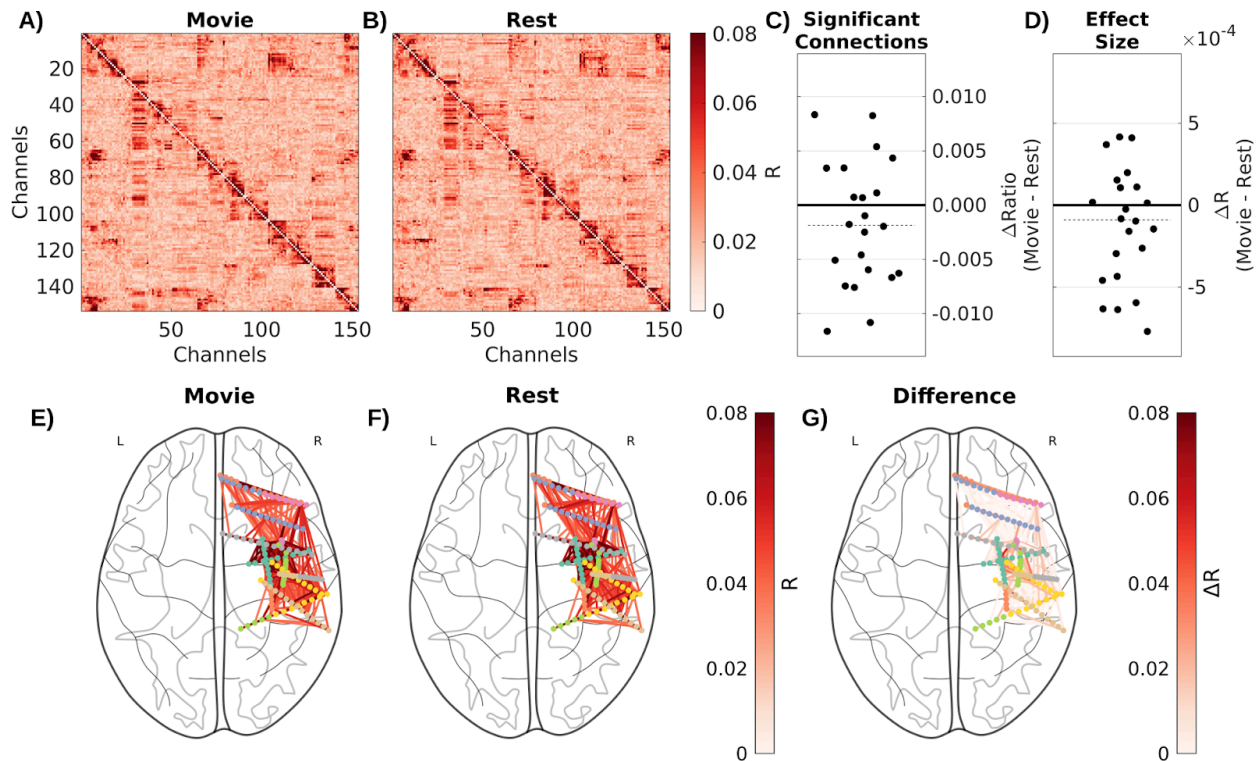
348 **Recurrent connectivity unchanged during movies and rest**

349

350 Next we compared intrinsic “connectivity” between movie watching and rest (Fig. 4A-D). In the
 351 rest condition subjects have a fixation cross on a gray background. This obviously reduces the
 352 size and number of saccades as compared to movie watching, but does not abolish them (Fig.
 353 S4). We therefore use a VARX model including fixation onset as extrinsic variable in both cases.
 354 Movies include film cuts and the sound envelope as external inputs. To control for the number of
 355 free parameters, we include copies of the film cut and sound envelope features from the movies
 356 to the resting state model. Remarkably, the number of significant recurrent connections in A
 357 were not detectably different between movie watching and rest (Fig. 4C, median=-0.0019,
 358 $p=0.19$, $N=22$, Wilcoxon), as is the effect size (Fig. 4D, median= -9×10^{-5} , $p=0.14$, $N=22$,
 359 Wilcoxon). One caveat to this conclusion is that the signal we analyzed was only 5 minutes long
 360 for the movie and rest conditions, and longer records may have revealed small differences.
 361 However, even on 5 minutes of data we observe a decrease in R values when including external

362 inputs (Fig. S5). Connectivity of BHA between movie and rest does also not differ significantly
 363 (Fig. S6). Using different segments of movies, in some cases we find a small reduction of
 364 significant connections in movie watching compared to resting state conditions (Fig. S7).
 365 However, overall, differences in the intrinsic connectivity between movie and rest, if they exist,
 366 are less systematic than the effect of the stimulus.

367



368

369 **Figure 4: Recurrent connectivity A during movies does not detectably differ from rest.** Effect size
 370 R for each connection in A . A) VARX model of 5 minutes of LFP recordings during movie watching, with
 371 sound envelope, fixation onsets and film cuts as input features. B) VARX model during resting fixation
 372 with fixation onset as input feature. C) Difference in the number of significant connections ($p < .0001$)
 373 between movie and rest. D) Difference in mean effect size across all channels between movie and rest.
 374 Dots represent subjects, dashed line the median across subjects. Axial view of significant connections in
 375 E) the movie task, F) resting state, and G) the difference between movies and resting state. Dots show
 376 the location of contacts in MNI space. Lines show significant connections between contacts. For plotting
 377 purposes connections in the upper triangle are plotted and asymmetries ignored. Only channels with
 378 p -values < 0.001 in both conditions are plotted.

379

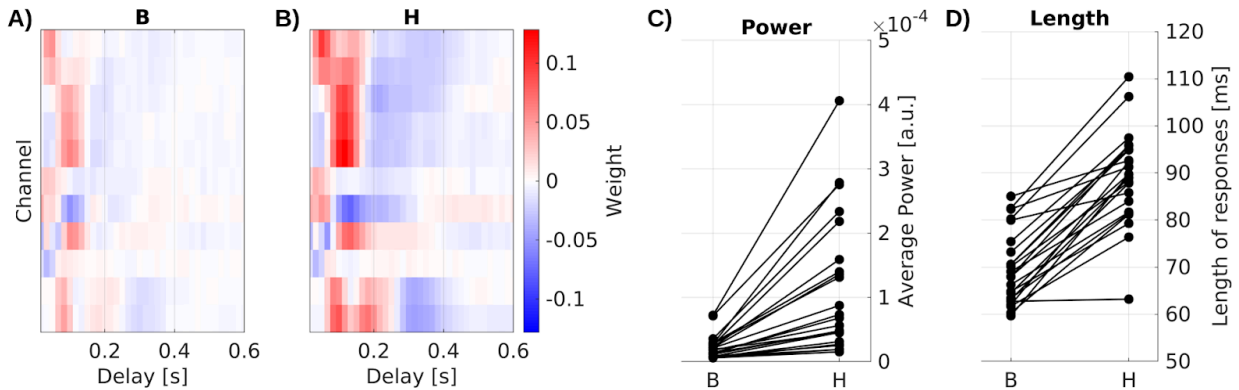
380

381 **Recurrent dynamic enhances and prolongs stimulus responses**

382

383 We also compared the immediate exogenous effect B with the total system response H , which
 384 includes the additional effect of the recurrent dynamic A . We estimate B with the VARX model
 385 (Fig. 5A) on data during video watching, and estimate the total response H directly using
 386 temporal response functions (Fig. 5B). Both models include fixation onset, film cuts and sound
 387 envelope as external inputs. We compare the power and length of filters from both models (Fig.

388 5C-D). We compare responses in channels with significant effects of **B** (FDR correction,
389 $\alpha=0.05$). We see that the total response **H** fixation onset is significantly stronger (Fig. 5C,
390 $\text{median}\Delta=-5.4*10^{-5}$, $p<.0001$, $N=23$, Wilcoxon) and longer than the immediate effect **B** (Fig.
391 5D, $\text{median}\Delta=-21.72\text{ms}$, $p<.0001$, $N=23$, Wilcoxon). The same effect is observed for other input
392 features and for BHA responses (Fig. S8). This suggests that the total response of the brain to
393 these external inputs is dominated by the recurrent dynamic of the brain.
394



396 **Figure 5: Impulse response models.** A) Immediate responses **B** to fixation onset are weaker and
397 shorter than B) the overall system response **H**. Significant responses of select channels in for one
398 example patient. C) Power and D) mean length of responses in significant channels for all patients. Each
399 line is a patient. Channels with the strongest responses are shown in panels A&B. Responses to fixation
400 onset in all significant channels, as well as auditory envelope and film cuts are shown in Figure S9.

401

402

403 **Results are similar for VARX models of BHA and LFP**

404

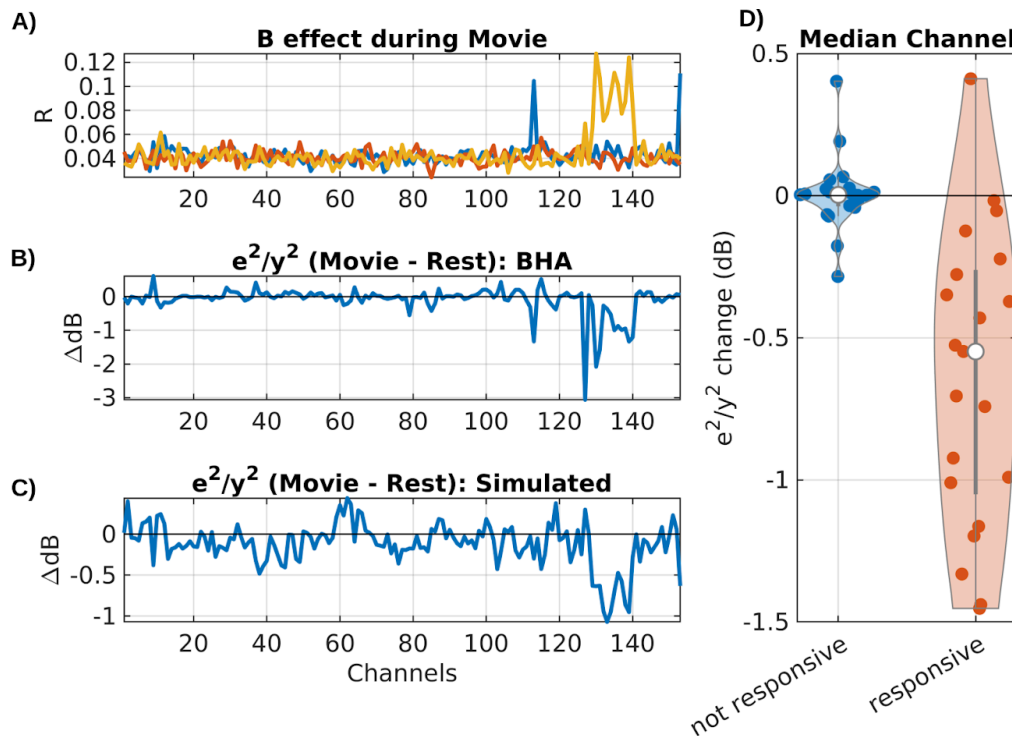
405 We repeated the same analyses of Figures 3-5 with broadband high frequency activity (BHA).
406 While LFP are thought to capture dendritic currents, BHA is correlated with neuronal firing rates
407 in the vicinity of an electrode. Generally we find a more sparse recurrent connectivity for BHA as
408 compared to LFP (compare Fig. 3&4 with Fig. S3&S6). Perhaps this is expected, given that LFP
409 covers a broader frequency range. Regardless of this overall difference, we find similar results
410 when analyzing BHA with the VARX model. Namely, taking the extrinsic input into account
411 removed stimulus-induced intrinsic “connections” (Fig. S3); the resulting model of the recurrent
412 dynamic is indistinguishable between watching movies and rest (Fig. S6); and responses to the
413 stimulus are stronger and more prolonged when separately modeling the effect of recurrent
414 connectivity (Fig. S8). In the Discussion section we will argue that some of these results are
415 expected in general when decomposing the total system response into extrinsic and intrinsic
416 effects. What we did not necessarily expect is that the intrinsic dynamics is similar during
417 movies and rest for both LFP and BHA.

418

419 ***Intrinsic “noise” in BHA is reduced by external stimulus***

420

421 So far we have discussed the mean response captured by \mathbf{B} and the recurrent activity
422 mediated by \mathbf{A} . We now want to analyze whether the external input modulates the variability of
423 the internal dynamic. As a metric of internal variability we measured the power of the intrinsic
424 innovation process $e^{(t)}$. For the LFP signal we see a drop in power during movies as
425 compared to rest, for both the original signal $\mathcal{Y}^{(t)}$ (Fig. S10A) and the model's innovation
426 process $e^{(t)}$ (Fig. S10B). Notable is the stronger oscillatory activity during rest (Fig. S10A). In
427 this example we see a drop in power in the theta/alpha band (5-11 Hz) during movie watching
428 across all electrodes (Fig. S10A, dotted lines). We observe similar narrow-band drop in power in
429 most patients, albeit at different frequencies (not shown). When analyzing BHA, we find no
430 difference in power of the innovation process between movie and rest, but we do find a drop in
431 power relative to the overall BHA signals for some channels (Fig. 6B). These channels seem to
432 coincide with channels that responded to the external stimuli, i.e. channels with a significant
433 effect in \mathbf{B} (Fig. 6A). If we take for each subject the median relative power for responsive
434 channels (median among those with $p < 0.0001$), then we find that relative power drops for nearly
435 all subjects (Fig 6D, Wilcoxon rank sum test, $p = 2.6e-06$, $N = 21$). The motivation for analyzing
436 only responsive channels comes from a simple gain adaptation (Fig. S11). Gain adaptation
437 keeps the power of $\mathcal{Y}^{(t)}$ constant, so that the extra power injected by the stimulus implicitly
438 reduces the relative power of the innovation process. This effect is specific to channels receiving
439 external input (Fig. S11D) and absent in a linear system without gain adaptation (Fig. S11C). To
440 demonstrate that this simple gain adaptation can explain the noise quenching in the neural data,
441 we simulated data with the gain adaptation model (Fig. 6C) using parameters estimated for the
442 example subject of Fig. 6A/B.



443

444 **Figure 6: For BHA, relative power of innovation vs signal drops during movies as compared to**
445 **rest in responsive channels.** A) Effect size R for extrinsic effect \mathbf{B} in all channels for 3 input features
446 (scene cuts, fixation onset, sound envelope). In this example 15 electrodes had significant responses to
447 one of the three inputs (Bonferroni corrected at $p < 0.01$). B) Change in relative power of innovation
448 (dB(innovation power / signal power), then subtracting movie - rest). C) Change in relative power of
449 innovation in a simulation of a VARX model with gain adaptation. Here we are using the \mathbf{A} and \mathbf{B} filters
450 that were estimated on BHA on the example from panel A and B. D) Median of power ratio change across
451 all subjects, contrasting responsive vs non-responsive channels.

452

453

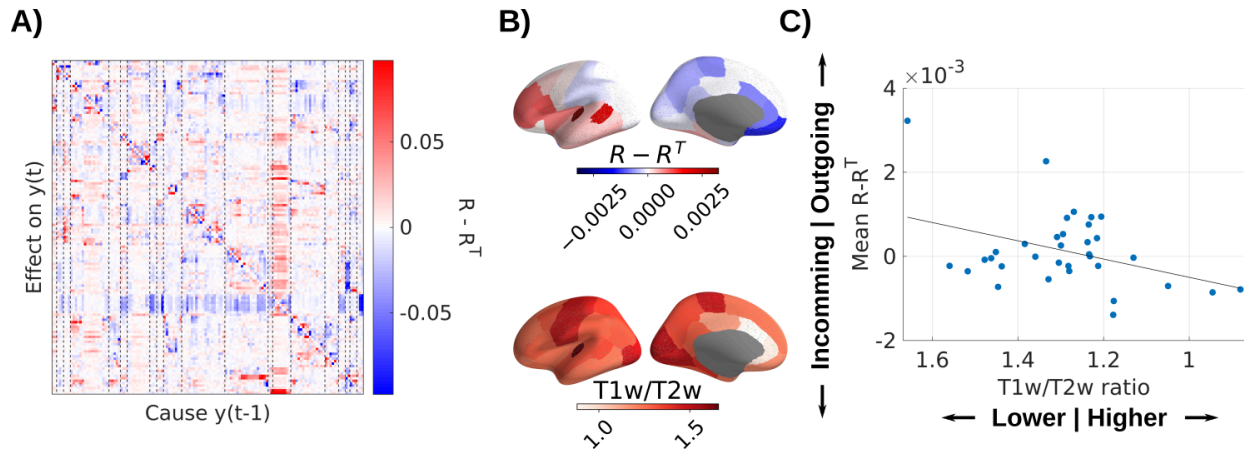
454 ***Direction of connectivity differs with cortical hierarchy***

455

456 Finally, we measured the directionality of the recurrent connections in the LFPs by analyzing the
457 structure of the resulting matrices R of all subjects. Columns in R represent outgoing
458 connections, while rows are incoming connections. Therefore, the difference of $R - R^T$ (Fig.
459 7A) averaged along a column has positive values if a node has overall stronger outgoing
460 connections, and negative values if it has stronger incoming connections. We measured this
461 directionality for each channel across all subjects and averaged also across channels within
462 parcels of the Desikan-Killiany atlas (N=35 regions of interest, Fig. 7B) ⁵⁸. We expected this to
463 co-vary with "cortical hierarchy". To test this, we compared this asymmetry metric with the
464 T1w/T2w ratio, which captures gray matter myelination and is used as an indirect measure of
465 cortical hierarchy ^{51,59}. We also average T1w/T2w ratio in the same parcels of the
466 Desikan-Killiany atlas (Fig. 7B). Cortical areas showing more outgoing connections ($R - R^T >$

467 0) have lower T1w/T2w ratio, which are located higher on the cortical hierarchy (Pearson's $r =$
468 0.39, $p = 0.023$, Fig. 7C). BHA analysis shows the same trend (Fig. S12).

469



470

471 **Figure 7: Recurrent connectivity of LFP is directed from sensory to higher-order areas.** A)
472 Difference of $R - R^T$ showing asymmetric directed effects. Dashed lines indicate regions of interest in
473 the Desikan-Killiany atlas. B) Mean directionality across patients and T1w/T2w ratio are averaged in
474 parcels of the Desikan-Killiany atlas. C) Mean directionality is correlated with cortical hierarchy, estimated
475 with the T1w/T2w hierarchy.

476

477

478 Discussion

479

480 Our results suggest that intrinsic dynamics are not substantially altered during watching movies
481 as compared to rest. Instead, the external stimulus reverberates in the recurrent network with
482 the same dynamic as during rest. The duration and magnitude of response is in large part a
483 result of this recurrent dynamic.

484

485

486 *Response to extrinsic input versus intrinsic dynamics*

487

488 Previous literature does often not distinguish between intrinsic connectivity and extrinsic effects.
489 As a result, similarities and differences between rest and stimulus conditions reported
490 previously, do not draw a firm conclusion as to whether “functional connectivity” is preserved,
491 e.g. ^{12,16}. By systematically factoring out the effect of the external input we conclude here that
492 the intrinsic dynamic is unaltered. If one fails to factor out the effect of the stimulus, one may
493 mistake the stimulus-induced correlations for changes in “functional connectivity”.

494

495 In this work we focused on “passive” tasks, i.e. resting with gaze on a fixation point, versus
496 watching movies without any associated tasks. We did not analyze data during an active task
497 requiring behavioral responses. The literature on active tasks emphasizes “state change” in
498 functional connectivity. ^{14,20,60} Efforts to factor out task-evoked activity when computing functional

499 connectivity concord with our conclusions that connectivity is inflated by a task¹⁷. Nevertheless,
500 we hesitate extrapolating our findings to active tasks, as we have not analyzed such data.

501

502 Conventional “encoding” models, such as temporal response functions, capture the total
503 response H of the brain to an external stimulus. Here we factored this into a moving average
504 filter B , followed by an autoregressive filter A . The important observation is that this intrinsic
505 dynamic governed by A does not change during stimulus processing. Arguably then, the role of
506 the initial responses B is to shape the input to be processed by the existing intrinsic dynamic.
507 This interpretation is consistent with the view of “the brain from the inside out” advocated by
508 György Buzsáki⁶¹. In this view, learning of a stimulus representation consists in learning a
509 mapping of the external stimulus to an existing intrinsic dynamic of the brain.

510

511

512 ***Similar findings for LFP and BHA***

513

514 We found a more sparse recurrent connectivity for BHA as compared to LFP. This may be
515 expected because correlations in lower frequencies (that dominate LFPs) reaches over longer
516 distances compared to correlations in higher frequencies (e.g. Muller et al., 2016). BHA has
517 been linked to a mixture of neuronal firing and dendritic currents⁶², in contrast to LFP, which is
518 thought to originate from widespread dendritic currents. Despite the observed differences in
519 sparsity, for both LFP and BHA we found that modeling the recurrent dynamic removed spurious
520 intrinsic connections. Removal of spurious effects when controlling for a common cause is a
521 generic finding in multivariate statistical models. We also found for both LFP and BHA that the
522 duration and strength of stimulus responses can be largely attributed to the recurrent dynamic.
523 Arguably, this is a generic feature of an autoregressive model, as it more readily captures longer
524 impulse responses. However, the extrinsic filters B in principle have an advantage as they can
525 be fit to each stimulus and brain location. In contrast, the recurrent filters A are constrained by
526 having to capture a shared dynamic for all stimulus dimensions. Thus, the predominance of the
527 recurrent dynamic in the total system response is not a trivial result of the factorization into
528 intrinsic and extrinsic effects. Finally, we did not necessarily expect that the intrinsic connectivity
529 is preserved between movie and rest in both LFP and BHA. This consistency may be due to a
530 variety of processes that are constant across conditions, such as internal thought, body and eye
531 movements. Active sensing through eye movements, for example, influences activity in a global
532 network^{63,64}, and likely accounts for part of the common source of correlations across
533 conditions.

534

535

536 ***Stimulus-induced reduction of noise in the intrinsic activity***

537

538 One difference we did find between LFP and BHA is the intrinsic innovation process, i.e. the
539 internal sources of variability or “noise”. For both BHA and LFP we saw a drop in the magnitude
540 of signal fluctuations during the movie watching condition. For the BHA but not the LFP, this was
541 explained as a drop in intrinsic noise. Specifically, for BHA there was less relative power in the
542 intrinsic “noise” for channels that are responsive to the stimulus. This is consistent with the

543 notion that response variability is due to variability of intrinsic activity²² which is found to
544 decrease across the brain with the onset of an external stimulus⁶⁵. This type of noise quenching
545 has been associated with increased attention⁶⁶ and improved visual discrimination performance
546⁶⁷. The effect we found here can be explained by a VARX model with the addition of a divisive
547 gain adaptation mechanism that keeps the total power of brain activity constant. When the input
548 injects additional power, this nonlinear gain adaptation implicitly reduces the contribution of the
549 intrinsic noise to the total power.

550

551 We also observed an overall drop in LFP power during movie watching. This phenomenon was
552 strongest in oscillatory bands, with frequencies in theta to beta band differing across subjects. In
553 scalp EEG, noise quenching is associated with a similar overall drop in power with the stimulus
554⁶⁶. This quenching of neural variability was also found to reduce correlation between brain areas
555 for fMRI and neural spiking²⁶. Both fMRI and neural spiking correlated with BHA⁶⁸. This is at
556 odds with our finding that intrinsic connectivity in BHA does not change significantly between
557 movie and rest. However, we can not rule out such differences on longer recordings.

558

559

560 ***Stimulus features***

561

562 During the movie and rest periods, we utilized fixation onset to capture activity that is
563 time-locked to visual processing because subjects move their eyes even during rest. We also
564 incorporated the sound envelope, a prominent feature known for capturing the dominant
565 audio-induced variance in scalp EEG³³. In addition, we included film cuts as features, as we
566 had previously demonstrated that they dominate the response in the BHA across the brain⁴⁸.
567 While other basic visual features such as overall optic flow or fixations on faces elicited
568 responses in the BHA, their contribution was relatively smaller. The analysis is not limited to
569 these few features, and future research should explore which stimulus features capture variance
570 in the data and how they affect the apparent intrinsic connectivity. There is a substantial body of
571 literature on encoding models of semantic features, where nonlinear features of a continuous
572 natural stimulus are extracted and then linearly regressed against fMRI^{69,70} or EEG⁷¹. This work
573 can be directly replicated with the VARX model which further models the intrinsic connectivity.

574

575

576 ***Alternative approaches***

577

578 The traditional VAR model has been used extensively in neuroscience to establish directed
579 “Granger causal” connections⁴¹. This approach has been very fruitful and found numerous
580 extensions, e.g.^{10,11}. However, these model implementations do not specifically account for an
581 external input.

582

583 A few methods have attempted to model the effect of varying task conditions on functional
584 connectivity, mostly in the analysis of fMRI. One approach is to first model the task-evoked
585 responses, equivalent to estimating \mathbf{B} alone, and then compute the conventional “functional
586 connectivity”, i.e. the correlation matrix, on the residuals $\mathbf{e}(t)$ ⁷². Others suggested to estimate \mathbf{B}

587 in multiple time windows and then estimate a “task related functional connectivity” by correlating
588 the multiple \mathbf{B} over time windows⁷³. It is not clear that these ad-hoc methods systematically
589 separate intrinsic from extrinsic factors.

590

591 A more principled modeling approach is “dynamic causal modeling” (DCM)¹⁹ and extensions
592 thereof⁷⁴. Similar to the VARX model, DCM includes intrinsic and extrinsic effects \mathbf{A} and \mathbf{B} .
593 However, the modeling is limited to first-order dynamics (i.e. $n_a=n_a=1$). Instead, the DCM
594 includes a multiplicative interaction of extrinsic input $\mathbf{x}(t)$ on the connectivity \mathbf{A} , which does not
595 exist in the VARX model. This interaction has been used to explicitly model a change in intrinsic
596 connectivity with task conditions. Here we found that this may not be necessary for intracranial
597 EEG. A practical advantage of the VARX model is the assumption that the neural activity is
598 directly observed. Instead, many existing models assume an error in the observations, which
599 triggers computationally intensive estimation algorithms, typically the expectation maximization
600 algorithm. The same is true for the “output error” model in linear systems theory²⁹. As a result,
601 these models are often limited to small networks⁶ to test specific alternative hypotheses⁴². In
602 contrast, here we have analyzed 100-200 channels per subject across the brain, and have
603 drawn more general conclusions about whole-brain activity.

604

605

606 **Caveats**

607

608 The lack of a significant difference in recurrent connectivity between stimulus and rest should be
609 interpreted with care. As usual, lack of evidence is not evidence for the lack of an effect. We
610 saw no change in the number of recurrent connections between movie and rest, either for the
611 LFPs or BHA activity. However, in individual movie segments small differences were observed
612 (Fig. S7). It is possible that regressing out a richer stimulus characterization would have
613 removed additional stimulus-induced correlation, only enhancing this small difference between
614 movie and rest. We were also limited to 5 minutes of data in the direct comparison of movie and
615 resting state data. Longer recordings might further enhance differences. Higher recurrent
616 connectivity in the LFP during rest would be consistent with the more synchronized state we
617 saw in rest, as reflected by larger oscillatory activity.

618

619 We find a correlation of DTI structural connectivity used in a model with a VARX estimate of
620 0.70. That is considered a relatively large value compared to other studies that attempt to
621 recover DTI connectivity from the correlation structure of fMRI activity⁴⁴. A Caveat is that this
622 was done on a biophysical model of firing rate, not fMRI, and we have not explored the
623 parameters of the model that might affect the results.

624

625 We used fixation onsets as external input, but it should be noted that they are tightly correlated
626 in time with saccade onsets (there is only about a 30 ms jitter between the two, depending on
627 saccade amplitude). While saccades are driven by visual movement, they are generated by the

628 ⁶ The original DCM proposed for fMRI included an added complication of modeling the
629 hemodynamic response, which amounts to adding a temporal filter to each output node and
630 prior to adding observation noise.

631 brain itself and arguably could also be seen as intrinsic. The same is true for all motor
632 behaviors, most of which cause a corresponding sensory response, similar to the visual
633 response following a saccade. Including them as external input is a modeling choice we have
634 made here, but it is important to acknowledge that fixation onsets can therefore have “acausal”
635 components⁴⁸. By “acausal” we mean a fixation-locked response that precedes the fixation
636 onset and is due to the neural activity leading up to the saccade and subsequent fixation. Such
637 acausal responses can be captured by the VARX Granger formalism by delaying the input
638 relative to the neural activity, which we have not done here.

639

640 The correlation between the average incoming and outgoing connections and cortical hierarchy
641 (Fig. 7) is not significant when normalizing for the number of electrodes in each region of
642 interest. Regions in the temporal lobe with a large number of electrodes might drive this
643 correlation. A more fine grained analysis in these regions could be the goal of future analysis.

644

645

646 **Conclusion**

647

648 We analyzed whole-brain intracranial recordings in human subjects at rest and while they
649 watched videos. We used a model that separates intrinsic dynamics from extrinsic effects. We
650 found that the recurrent dynamic observed during rest is largely unaltered when watching
651 movies. Instead, the brain's response to the audiovisual stimuli appears to be substantially
652 shaped by its endogenous dynamic. The reduction in intrinsic variance observed during an
653 extrinsic stimulus may be the result of neuronal gain adaptation.

654

655 **Acknowledgements**

656

657 We would like to thank Chris Honey for advice on the model validation with simulations and
658 related references. We like to thank Behtash Babadi for help on the development of the Granger
659 formalism for the VARX model. This work was supported in part by the NIH through grants P50
660 MH109429 and R01DC019979.

661

662

663 **Author contributions**

664

665 Conceptualization, L.C.P. and M.N.; Methodology, L.C.P.; Software, L.C.P. and M.N.; Formal
666 Analysis: M.N. and L.C.P.; Investigation, M.N. and M.L.; Resources, S.B.; Writing – Original
667 Draft, L.C.P. and M.N.; Writing – Review & Editing, L.C.P., M.N., M.L., C.E.S., S.B.; Funding
668 Acquisition, L.C.P., C.E.S. and S.B.; Visualization, M.N.; Supervision, L.C.P., C.E.S., S.B.

669

670

671 **Declaration of interests**

672

673 The authors declare no competing interests.

674

675

676 **Supplemental information**

677

678 Figures S1–S12 and Table S1

679 References

680

- 681 1. Felleman, D.J., and Van Essen, D.C. (1991). Distributed Hierarchical Processing in the
682 Primate Cerebral Cortex. *Cereb. Cortex* 1, 1–47. <https://doi.org/10.1093/cercor/1.1.1-a>.
- 683 2. Friston, K.J., Holmes, A.P., Poline, J.-B., Grasby, P.J., Williams, S.C.R., Frackowiak, R.S.J.,
684 and Turner, R. (1995). Analysis of fMRI Time-Series Revisited. *NeuroImage* 2, 45–53.
685 <https://doi.org/10.1006/nimg.1995.1007>.
- 686 3. Lalor, E.C., and Foxe, J.J. (2010). Neural responses to uninterrupted natural speech can be
687 extracted with precise temporal resolution. *Eur. J. Neurosci.* 31, 189–193.
688 <https://doi.org/10.1111/j.1460-9568.2009.07055.x>.
- 689 4. Greicius, M.D., Krasnow, B., Reiss, A.L., and Menon, V. (2003). Functional connectivity in
690 the resting brain: A network analysis of the default mode hypothesis. *Proc. Natl. Acad. Sci.*
691 100, 253–258. <https://doi.org/10.1073/pnas.0135058100>.
- 692 5. Varela, F., Lachaux, J.-P., Rodriguez, E., and Martinerie, J. (2001). The brainweb: Phase
693 synchronization and large-scale integration. *Nat. Rev. Neurosci.* 2, 229–239.
694 <https://doi.org/10.1038/35067550>.
- 695 6. Friston, K., Moran, R., and Seth, A.K. (2013). Analysing connectivity with Granger causality
696 and dynamic causal modelling. *Curr. Opin. Neurobiol.* 23, 172–178.
697 <https://doi.org/10.1016/j.conb.2012.11.010>.
- 698 7. Haufe, S., Nikulin, V.V., Müller, K.-R., and Nolte, G. (2013). A critical assessment of
699 connectivity measures for EEG data: A simulation study. *NeuroImage* 64, 120–133.
700 <https://doi.org/10.1016/j.neuroimage.2012.09.036>.
- 701 8. Pellegrini, F., Delorme, A., Nikulin, V., and Haufe, S. (2023). Identifying good practices for
702 detecting inter-regional linear functional connectivity from EEG. *NeuroImage* 277, 120218.
703 <https://doi.org/10.1016/j.neuroimage.2023.120218>.
- 704 9. Seth, A.K., Barrett, A.B., and Barnett, L. (2015). Granger Causality Analysis in
705 Neuroscience and Neuroimaging. *J. Neurosci.* 35, 3293–3297.
706 <https://doi.org/10.1523/JNEUROSCI.4399-14.2015>.
- 707 10. Sheikhattar, A., Miran, S., Liu, J., Fritz, J.B., Shamma, S.A., Kanold, P.O., and Babadi, B.
708 (2018). Extracting neuronal functional network dynamics via adaptive Granger causality
709 analysis. *Proc. Natl. Acad. Sci.* 115, E3869–E3878.
710 <https://doi.org/10.1073/pnas.1718154115>.
- 711 11. Soleimani, B., Das, P., Dushyanthi Karunathilake, I.M., Kuchinsky, S.E., Simon, J.Z., and
712 Babadi, B. (2022). NLGC: Network localized Granger causality with application to MEG
713 directional functional connectivity analysis. *NeuroImage* 260, 119496.
714 <https://doi.org/10.1016/j.neuroimage.2022.119496>.
- 715 12. Betti, V., Della Penna, S., de Pasquale, F., Mantini, D., Marzetti, L., Romani, G.L., and
716 Corbetta, M. (2013). Natural Scenes Viewing Alters the Dynamics of Functional Connectivity
717 in the Human Brain. *Neuron* 79, 782–797. <https://doi.org/10.1016/j.neuron.2013.06.022>.
- 718 13. Geerligs, L., Rubinov, M., Cam-CAN, and Henson, R.N. (2015). State and Trait Components
719 of Functional Connectivity: Individual Differences Vary with Mental State. *J. Neurosci.* 35,
720 13949–13961. <https://doi.org/10.1523/JNEUROSCI.1324-15.2015>.
- 721 14. Mennes, M., Kelly, C., Colcombe, S., Castellanos, F.X., and Milham, M.P. (2013). The
722 Extrinsic and Intrinsic Functional Architectures of the Human Brain Are Not Equivalent.
723 *Cereb. Cortex* 23, 223–229. <https://doi.org/10.1093/cercor/bhs010>.
- 724 15. Vanderwal, T., Eilbott, J., Finn, E.S., Craddock, R.C., Turnbull, A., and Castellanos, F.X.
725 (2017). Individual differences in functional connectivity during naturalistic viewing conditions.
726 *NeuroImage* 157, 521–530. <https://doi.org/10.1016/j.neuroimage.2017.06.027>.
- 727 16. Demirtaş, M., Ponce-Alvarez, A., Gilson, M., Hagmann, P., Mantini, D., Betti, V., Romani,
728 G.L., Friston, K., Corbetta, M., and Deco, G. (2019). Distinct modes of functional

- connectivity induced by movie-watching. *NeuroImage* 184, 335–348.
<https://doi.org/10.1016/j.neuroimage.2018.09.042>.
17. Cole, M.W., Ito, T., Schultz, D., Mill, R., Chen, R., and Cocuzza, C. (2019). Task activations produce spurious but systematic inflation of task functional connectivity estimates. *NeuroImage* 189, 1–18. <https://doi.org/10.1016/j.neuroimage.2018.12.054>.
18. Pearl, J. (2013). Linear Models: A Useful “Microscope” for Causal Analysis. *J. Causal Inference* 1, 155–170. <https://doi.org/10.1515/jci-2013-0003>.
19. Friston, K.J., Harrison, L., and Penny, W. (2003). Dynamic causal modelling. *NeuroImage* 19, 1273–1302. [https://doi.org/10.1016/S1053-8119\(03\)00202-7](https://doi.org/10.1016/S1053-8119(03)00202-7).
20. Gonzalez-Castillo, J., and Bandettini, P.A. (2018). Task-based dynamic functional connectivity: Recent findings and open questions. *NeuroImage* 180, 526–533. <https://doi.org/10.1016/j.neuroimage.2017.08.006>.
21. Fox, M.D., Snyder, A.Z., Zacks, J.M., and Raichle, M.E. (2006). Coherent spontaneous activity accounts for trial-to-trial variability in human evoked brain responses. *Nat. Neurosci.* 9, 23–25. <https://doi.org/10.1038/nn1616>.
22. Arieli, A., Sterkin, A., Grinvald, A., and Aertsen, A. (1996). Dynamics of Ongoing Activity: Explanation of the Large Variability in Evoked Cortical Responses. *Science* 273, 1868–1871. <https://doi.org/10.1126/science.273.5283.1868>.
23. Buzsaki, G. (2006). *Rhythms of the Brain* (Oxford University Press).
24. Fiser, J., Chiu, C., and Weliky, M. (2004). Small modulation of ongoing cortical dynamics by sensory input during natural vision. *Nature* 431, 573–578. <https://doi.org/10.1038/nature02907>.
25. Gray, C.M., König, P., Engel, A.K., and Singer, W. (1989). Oscillatory responses in cat visual cortex exhibit inter-columnar synchronization which reflects global stimulus properties. *Nature* 338, 334–337. <https://doi.org/10.1038/338334a0>.
26. Ito, T., Brincat, S.L., Siegel, M., Mill, R.D., He, B.J., Miller, E.K., Rotstein, H.G., and Cole, M.W. (2020). Task-evoked activity quenches neural correlations and variability across cortical areas. *PLOS Comput. Biol.* 16, e1007983. <https://doi.org/10.1371/journal.pcbi.1007983>.
27. Nauhaus, I., Busse, L., Carandini, M., and Ringach, D.L. (2009). Stimulus contrast modulates functional connectivity in visual cortex. *Nat. Neurosci.* 12, 70–76. <https://doi.org/10.1038/nn.2232>.
28. Roelfsema, P.R., Engel, A.K., König, P., and Singer, W. (1997). Visuomotor integration is associated with zero time-lag synchronization among cortical areas. *Nature* 385, 157–161. <https://doi.org/10.1038/385157a0>.
29. Ljung, L. (1999). *System Identification: Theory for the User* (Prentice Hall PTR).
30. Hamilton, J.D. (2020). *Time Series Analysis* (Princeton University Press).
31. Parra, L.C., Silvan, A., Nentwich, M., Madsen, J., and Babadi, B. (2024). *VARX Granger Analysis: Modeling, Inference, and Applications*. Preprint at arXiv.
32. Naselaris, T., Kay, K.N., Nishimoto, S., and Gallant, J.L. (2011). Encoding and decoding in fMRI. *NeuroImage* 56, 400–410. <https://doi.org/10.1016/j.neuroimage.2010.07.073>.
33. Di Liberto, G.M., O’Sullivan, J.A., and Lalor, E.C. (2015). Low-Frequency Cortical Entrainment to Speech Reflects Phoneme-Level Processing. *Curr. Biol.* 25, 2457–2465. <https://doi.org/10.1016/j.cub.2015.08.030>.
34. Holdgraf, C.R., Rieger, J.W., Micheli, C., Martin, S., Knight, R.T., and Theunissen, F.E. (2017). Encoding and Decoding Models in Cognitive Electrophysiology. *Front. Syst. Neurosci.* 11. <https://doi.org/10.3389/fnsys.2017.00061>.
35. Li, Y., Anumanchipalli, G.K., Mohamed, A., Chen, P., Carney, L.H., Lu, J., Wu, J., and Chang, E.F. (2023). Dissecting neural computations in the human auditory pathway using deep neural networks for speech. *Nat. Neurosci.*, 1–13. <https://doi.org/10.1038/s41593-023-01468-4>.

- 780 36. Granger, C.W.J. (1969). Investigating Causal Relations by Econometric Models and
781 Cross-spectral Methods. *Econometrica* 37, 424–438. <https://doi.org/10.2307/1912791>.
- 782 37. Geweke, J. (1982). Measurement of Linear Dependence and Feedback between Multiple
783 Time Series. *J. Am. Stat. Assoc.* 77, 304–313.
784 <https://doi.org/10.1080/01621459.1982.10477803>.
- 785 38. Magee, L. (1990). R² Measures Based on Wald and Likelihood Ratio Joint Significance
786 Tests. *Am. Stat.* 44, 250–253. <https://doi.org/10.1080/00031305.1990.10475731>.
- 787 39. Crosse, M.J., Di Liberto, G.M., Bednar, A., and Lalor, E.C. (2016). The Multivariate Temporal
788 Response Function (mTRF) Toolbox: A MATLAB Toolbox for Relating Neural Signals to
789 Continuous Stimuli. *Front. Hum. Neurosci.* 10. <https://doi.org/10.3389/fnhum.2016.00604>.
- 790 40. Friston, K.J., Holmes, A.P., Worsley, K.J., Poline, J.-P., Frith, C.D., and Frackowiak, R.S.J.
791 (1994). Statistical parametric maps in functional imaging: A general linear approach. *Hum.*
792 *Brain Mapp.* 2, 189–210. <https://doi.org/10.1002/hbm.460020402>.
- 793 41. Barnett, L., and Seth, A.K. (2014). The MVGC multivariate Granger causality toolbox: A new
794 approach to Granger-causal inference. *J. Neurosci. Methods* 223, 50–68.
795 <https://doi.org/10.1016/j.jneumeth.2013.10.018>.
- 796 42. Penny, W.D., Stephan, K.E., Mechelli, A., and Friston, K.J. (2004). Comparing dynamic
797 causal models. *NeuroImage* 22, 1157–1172.
798 <https://doi.org/10.1016/j.neuroimage.2004.03.026>.
- 799 43. Cakan, C., Jajcay, N., and Obermayer, K. (2023). neurolib: A Simulation Framework for
800 Whole-Brain Neural Mass Modeling. *Cogn. Comput.* 15, 1132–1152.
801 <https://doi.org/10.1007/s12559-021-09931-9>.
- 802 44. Honey, C.J., Sporns, O., Cammoun, L., Gigandet, X., Thiran, J.P., Meuli, R., and Hagmann,
803 P. (2009). Predicting human resting-state functional connectivity from structural connectivity.
804 *Proc. Natl. Acad. Sci.* 106, 2035–2040. <https://doi.org/10.1073/pnas.0811168106>.
- 805 45. Smith, S.M., Miller, K.L., Salimi-Khorshidi, G., Webster, M., Beckmann, C.F., Nichols, T.E.,
806 Ramsey, J.D., and Woolrich, M.W. (2011). Network modelling methods for FMRI.
807 *NeuroImage* 54, 875–891. <https://doi.org/10.1016/j.neuroimage.2010.08.063>.
- 808 46. Chen, X. (2023). xiaohuichen88/Graphical-Lasso.
- 809 47. Friedman, J., Hastie, T., and Tibshirani, R. (2008). Sparse inverse covariance estimation
810 with the graphical lasso. *Biostatistics* 9, 432–441.
811 <https://doi.org/10.1093/biostatistics/kxm045>.
- 812 48. Nentwich, M., Leszczynski, M., Russ, B.E., Hirsch, L., Markowitz, N., Sapru, K., Schroeder,
813 C.E., Mehta, A.D., Bickel, S., and Parra, L.C. (2023). Semantic novelty modulates neural
814 responses to visual change across the human brain. *Nat. Commun.* 14, 2910.
815 <https://doi.org/10.1038/s41467-023-38576-5>.
- 816 49. Vanderwal, T., Kelly, C., Eilbott, J., Mayes, L.C., and Castellanos, F.X. (2015). Inscapes : A
817 movie paradigm to improve compliance in functional magnetic resonance imaging.
818 *NeuroImage* 122, 222–232. <https://doi.org/10.1016/j.neuroimage.2015.07.069>.
- 819 50. Chamma, A., Frau-Pascual, A., Rothberg, A., Abadie, A., Abraham, A., Gramfort, A., Savio,
820 A., Cionca, A., Thual, A., Kodibagkar, A., et al. (2024). nilearn. Version 0.10.4 (Zenodo).
821 <https://doi.org/10.5281/zenodo.10948303> <https://doi.org/10.5281/zenodo.10948303>.
- 822 51. Gao, R., van den Brink, R.L., Pfeffer, T., and Voytek, B. (2020). Neuronal timescales are
823 functionally dynamic and shaped by cortical microarchitecture. *eLife* 9, e61277.
824 <https://doi.org/10.7554/eLife.61277>.
- 825 52. Gao, R., Voytek, B., and Olayinka, T. (2020). rdgao/field-echos: post-publication. Version
826 v1.0 (Zenodo). <https://doi.org/10.5281/zenodo.4362645>
827 <https://doi.org/10.5281/zenodo.4362645>.
- 828 53. Glasser, M.F., Coalson, T.S., Robinson, E.C., Hacker, C.D., Harwell, J., Yacoub, E., Ugurbil,
829 K., Andersson, J., Beckmann, C.F., Jenkinson, M., et al. (2016). A multi-modal parcellation
830 of human cerebral cortex. *Nature* 536, 171–178. <https://doi.org/10.1038/nature18933>.

- 831 54. Markello, R., Hansen, J., Liu, Z.-Q., Bazinet, V., Shafiei, G., Suarez, L., and Mišić, B. (2024).
832 neuromaps: structural and functional interpretation of brain maps. Version 0.0.5 (Zenodo).
833 <https://doi.org/10.5281/zenodo.10607923> <https://doi.org/10.5281/zenodo.10607923>.
- 834 55. Markello, R.D., Hansen, J.Y., Liu, Z.-Q., Bazinet, V., Shafiei, G., Suárez, L.E., Blstein, N.,
835 Seidlitz, J., Baillet, S., Satterthwaite, T.D., et al. (2022). neuromaps: structural and functional
836 interpretation of brain maps. *Nat. Methods* 19, 1472–1479.
837 <https://doi.org/10.1038/s41592-022-01625-w>.
- 838 56. Robinson, E.C., Garcia, K., Glasser, M.F., Chen, Z., Coalson, T.S., Makropoulos, A., Bozek,
839 J., Wright, R., Schuh, A., Webster, M., et al. (2018). Multimodal surface matching with
840 higher-order smoothness constraints. *NeuroImage* 167, 453–465.
841 <https://doi.org/10.1016/j.neuroimage.2017.10.037>.
- 842 57. Robinson, E.C., Jbabdi, S., Glasser, M.F., Andersson, J., Burgess, G.C., Harms, M.P.,
843 Smith, S.M., Van Essen, D.C., and Jenkinson, M. (2014). MSM: A new flexible framework
844 for Multimodal Surface Matching. *NeuroImage* 100, 414–426.
845 <https://doi.org/10.1016/j.neuroimage.2014.05.069>.
- 846 58. Desikan, R.S., Ségonne, F., Fischl, B., Quinn, B.T., Dickerson, B.C., Blacker, D., Buckner,
847 R.L., Dale, A.M., Maguire, R.P., Hyman, B.T., et al. (2006). An automated labeling system
848 for subdividing the human cerebral cortex on MRI scans into gyral based regions of interest.
849 *NeuroImage* 31, 968–980. <https://doi.org/10.1016/j.neuroimage.2006.01.021>.
- 850 59. Wang, X.-J. (2020). Macroscopic gradients of synaptic excitation and inhibition in the
851 neocortex. *Nat. Rev. Neurosci.* 21, 169–178. <https://doi.org/10.1038/s41583-020-0262-x>.
- 852 60. Cole, M.W., Bassett, D.S., Power, J.D., Braver, T.S., and Petersen, S.E. (2014). Intrinsic and
853 Task-Evoked Network Architectures of the Human Brain. *Neuron* 83, 238–251.
854 <https://doi.org/10.1016/j.neuron.2014.05.014>.
- 855 61. Buzsáki, G. (2019). *The Brain from Inside Out* (Oxford University Press).
- 856 62. Leszczyński, M., Barczak, A., Kajikawa, Y., Ulbert, I., Falchier, A.Y., Tal, I., Haegens, S.,
857 Melloni, L., Knight, R.T., and Schroeder, C.E. (2020). Dissociation of broadband
858 high-frequency activity and neuronal firing in the neocortex. *Sci. Adv.* 6, eabb0977.
859 <https://doi.org/10.1126/sciadv.abb0977>.
- 860 63. Leszczynski, M., Bickel, S., Nentwich, M., Russ, B.E., Parra, L., Lakatos, P., Mehta, A., and
861 Schroeder, C.E. (2023). Saccadic modulation of neural excitability in auditory areas of the
862 neocortex. *Curr. Biol.* <https://doi.org/10.1016/j.cub.2023.02.018>.
- 863 64. Leszczynski, M., Chaieb, L., Staudigl, T., Enkirch, S.J., Fell, J., and Schroeder, C.E. (2021).
864 Neural activity in the human anterior thalamus during natural vision. *Sci. Rep.* 11, 17480.
865 <https://doi.org/10.1038/s41598-021-96588-x>.
- 866 65. Churchland, M.M., Yu, B.M., Cunningham, J.P., Sugrue, L.P., Cohen, M.R., Corrado, G.S.,
867 Newsome, W.T., Clark, A.M., Hosseini, P., Scott, B.B., et al. (2010). Stimulus onset
868 quenches neural variability: a widespread cortical phenomenon. *Nat. Neurosci.* 13,
869 369–378. <https://doi.org/10.1038/nn.2501>.
- 870 66. Arazi, A., Yeshurun, Y., and Dinstein, I. (2019). Neural Variability Is Quenched by Attention.
871 *J. Neurosci.* 39, 5975–5985. <https://doi.org/10.1523/JNEUROSCI.0355-19.2019>.
- 872 67. Arazi, A., Censor, N., and Dinstein, I. (2017). Neural Variability Quenching Predicts
873 Individual Perceptual Abilities. *J. Neurosci.* 37, 97–109.
874 <https://doi.org/10.1523/JNEUROSCI.1671-16.2016>.
- 875 68. Mukamel, R., Gelbard, H., Arieli, A., Hasson, U., Fried, I., and Malach, R. (2005). Coupling
876 Between Neuronal Firing, Field Potentials, and fMRI in Human Auditory Cortex. *Science*
877 309, 951–954. <https://doi.org/10.1126/science.1110913>.
- 878 69. Huth, A.G., de Heer, W.A., Griffiths, T.L., Theunissen, F.E., and Gallant, J.L. (2016). Natural
879 speech reveals the semantic maps that tile human cerebral cortex. *Nature* 532, 453–458.
880 <https://doi.org/10.1038/nature17637>.
- 881 70. Nishimoto, S., Vu, A.T., Naselaris, T., Benjamini, Y., Yu, B., and Gallant, J.L. (2011).

- 882 Reconstructing Visual Experiences from Brain Activity Evoked by Natural Movies. *Curr. Biol.*
883 *21*, 1641–1646. <https://doi.org/10.1016/j.cub.2011.08.031>.
- 884 71. Broderick, M.P., Anderson, A.J., Di Liberto, G.M., Crosse, M.J., and Lalor, E.C. (2018).
885 Electrophysiological Correlates of Semantic Dissimilarity Reflect the Comprehension of
886 Natural, Narrative Speech. *Curr. Biol.* *28*, 803-809.e3.
887 <https://doi.org/10.1016/j.cub.2018.01.080>.
- 888 72. Fair, D.A., Schlaggar, B.L., Cohen, A.L., Miezin, F.M., Dosenbach, N.U.F., Wenger, K.K.,
889 Fox, M.D., Snyder, A.Z., Raichle, M.E., and Petersen, S.E. (2007). A method for using
890 blocked and event-related fMRI data to study “resting state” functional connectivity.
891 *NeuroImage* *35*, 396–405. <https://doi.org/10.1016/j.neuroimage.2006.11.051>.
- 892 73. Rissman, J., Gazzaley, A., and D’Esposito, M. (2004). Measuring functional connectivity
893 during distinct stages of a cognitive task. *NeuroImage* *23*, 752–763.
894 <https://doi.org/10.1016/j.neuroimage.2004.06.035>.
- 895 74. Ryali, S., Supekar, K., Chen, T., and Menon, V. (2011). Multivariate dynamical systems
896 models for estimating causal interactions in fMRI. *NeuroImage* *54*, 807–823.
897 <https://doi.org/10.1016/j.neuroimage.2010.09.052>.